



DOI: 10.5604/01.3001.0014.8189

# Thermal characterization of halloysite materials for porous ceramic preforms



M. Kujawa <sup>a,\*</sup>, R. Suwak <sup>a</sup>, L.A. Dobrzański <sup>b</sup>, A. Gerle <sup>a</sup>, B. Tomiczek <sup>c</sup>

<sup>a</sup> Łukasiewicz - Institute of Ceramics and Building Materials, Refractory Materials Division in Gliwice, ul. Toszecka 99, 44-100 Gliwice, Poland

<sup>b</sup> Medical and Dental Engineering Centre for Research, Design and Production ASKLEPIOS, ul. Królowej Bony 13 D, 44-100 Gliwice, Poland

<sup>c</sup> Division of Engineering Materials and Biomaterials, Silesian University of Technology, ul. Konarskiego 18a, 44-100 Gliwice, Poland

\* Corresponding e-mail address: magdalena.kujawa@icimb.lukasiewicz.gov.pl

ORCID identifier:  <https://orcid.org/0000-0002-9997-159X> (M.K.);  <https://orcid.org/0000-0002-7584-8917> (L.A.D.)

## ABSTRACT

**Purpose:** The aim of the study was to investigate the possibility of sintering raw (natural) halloysite and pure halloysite to produce porous ceramic preforms, and determination of sintering temperature based on the results of investigations into thermal effects, linear changes and phase transitions.

**Design/methodology/approach:** Due to mullitisation ability of halloysite at high temperature, alternative applications based on the sintering technology (including the production of reinforcement of metal matrix composites) are being searched for. Pure halloysite and Dunino halloysite were selected for the study.

**Findings:** Pure halloysite, characterized by low impurities, dimensional stability during sintering, softening temperature above 1500°C and ability to transform into mullite at temperatures above 950°C could be used as a base for the production of sintered, porous mullite preforms.

**Research limitations/implications:** Presence of impurities in Dunino halloysite, contribute to the shift of the sintering temperature towards lower temperatures and caused a rapid and uncontrolled shrinkage of the sample and the appearance of the softening temperature at 1300°C.

**Practical implications:** Based on the research of thermal (DTA/TG, linear changes in high-temperature microscopy) and XRD studies it is possible to determine the sintering temperature of pure halloysite to manufacture the porous mullite preforms with open porosity.

**Originality/value:** The received results show the possibility of obtaining the new mullite preforms based on pure halloysite.

**Keywords:** Halloysite, DTA/TG, XRD, High-temperature microscope, Linear changes

**Reference to this paper should be given in the following way:**

M. Kujawa, R. Suwak, L.A. Dobrzański, A. Gerle, B. Tomiczek, Thermal characterization of halloysite materials for porous ceramic preforms, Archives of Materials Science and Engineering 107/1 (2021) 5-15. DOI: <https://doi.org/10.5604/01.3001.0014.8189>

## MATERIALS

## 1. Introduction

Among the materials that are commonly used for elements exposed to high temperatures or abrasive wear e.g. in the automotive and aviation industries, special attention should be paid to metal matrix composites (MMCs) manufactured using infiltration methods [1-5]. The reinforcement of these materials, or local reinforcement of the finished product, results from the addition of molecules and short fibres into the matrix, having a form of porous ceramic preforms or foams with an open porosity of 60-90% [1, 5-13].

The type of reinforcement has an impact on the final cost of the composite material, so searches are undertaken to find slow-cost and easily accessible raw materials which in suitable thermal conditions provide reinforcement with high thermal stability, high corrosion resistance and low coefficient of thermal expansion and thermal conductivity, which is however comparable to that of the matrix material. The material meeting these criteria is be mullite, while aluminosilicate such as kaolinite, halloysite or montmorillonite can be used as the raw material to obtain it. These raw materials, due to their availability and ability to mullitize under appropriate thermal conditions [14-22], could be used as reinforcement of composite materials.

Due to its chemical composition, structural transformations during heating and a very small content of impurities (especially iron, titanium and calcium oxides) in comparison with raw halloysite, pure halloysite in the form of extracted nanotubes could be used as a base for the production of sintered, porous mullite preforms. Since pure halloysite has the ability to mullitize at high temperatures, searches are undertaken to find alternative applications based on the sintering technology, including the production of metal matrix composites [12, 23-25], while taking into account the potential influence of their nanometric dimension on the velocity of mullite formation [19].

Optimisation of the sintering temperature of ceramic materials is important for shaping their structural and strength properties. Since the melting point of mullite is approx. 1840°C (it depends on the ratio of Al<sub>2</sub>O<sub>3</sub> to SiO<sub>2</sub>) [17], and free sintering in the solid phase of the mullitisation reagents should take place at the temperature of ca 0.5-0.8 mullite melting temperature, it is assumed that free sintering of halloysite should occur within the temperature range of 920°C-1472°C [26,27]. The sintering temperature affects the structure of ceramic sinter formed from the material containing halloysite. Therefore, to optimize the sintering temperature, thermal investigations complemented with a phase analysis have been proposed.

The aim of the study was to confirm the possibility of using halloysite in the form of sintered, porous ceramic preforms as reinforcement of aluminium matrix composites. The ability of pure halloysite to mullitize in the process of free sintering in a selected temperature range was investigated using thermal and phase composition studies.

## 2. Materials and methodology

### 2.1. Materials

The following were selected for the research: pure halloysite (nanotubes – HNT) supplied by NaturalNano (USA), raw halloysite Dunino supplied by Intermark, as the pore forming agent – carbon fibres (CF) Sigrafil C10 M250 UNS provided by SGL Carbon Group (in an amount of 30 wt.% or 50 wt.%) and 1 wt.% microwax. The morphology of the halloysites and carbon fibres is shown in Figure 1.

Pure halloysite is a nanotube extracted from natural halloysite, which has a form of a cylindrical object with a diameter below 100 nm and a length of 500 nm to over 1.2 µm, whereas Dunino halloysite has a lamellar-tube structure with visible halloysite nanotubes [28-30]. The chemical composition of pure halloysite and Dunino halloysite is presented in Table 1 (measurement uncertainty ±0.5 wt.%). Both materials differ in the content of Fe<sub>2</sub>O<sub>3</sub>, TiO<sub>2</sub>, CaO, MgO, K<sub>2</sub>O. These compounds are treated as impurities affecting the sintering temperature and increasing the amount of liquid phase and grain growth [31-33]. The content of these contaminants is much higher in Dunino halloysite.

Table 1.  
Chemical composition of pure and Dunino halloysite in delivery condition

	Mean mass concentration of elements, wt.%	
	HNT	DUNINO
Loss on ignition 1025°C	15.58	15.10
SiO <sub>2</sub>	45.63	41.77
Al <sub>2</sub> O <sub>3</sub>	37.93	34.23
Fe <sub>complete</sub> converted to Fe <sub>2</sub> O <sub>3</sub>	0.46	6.23
TiO <sub>2</sub>	0.11	1.23
CaO	0.01	0.43
MgO	0.07	0.15
K <sub>2</sub> O	0.01	0.14
Na <sub>2</sub> O	0.03	0.03
P <sub>2</sub> O <sub>5</sub>	0.35	0.45
Total	100.18	99.76

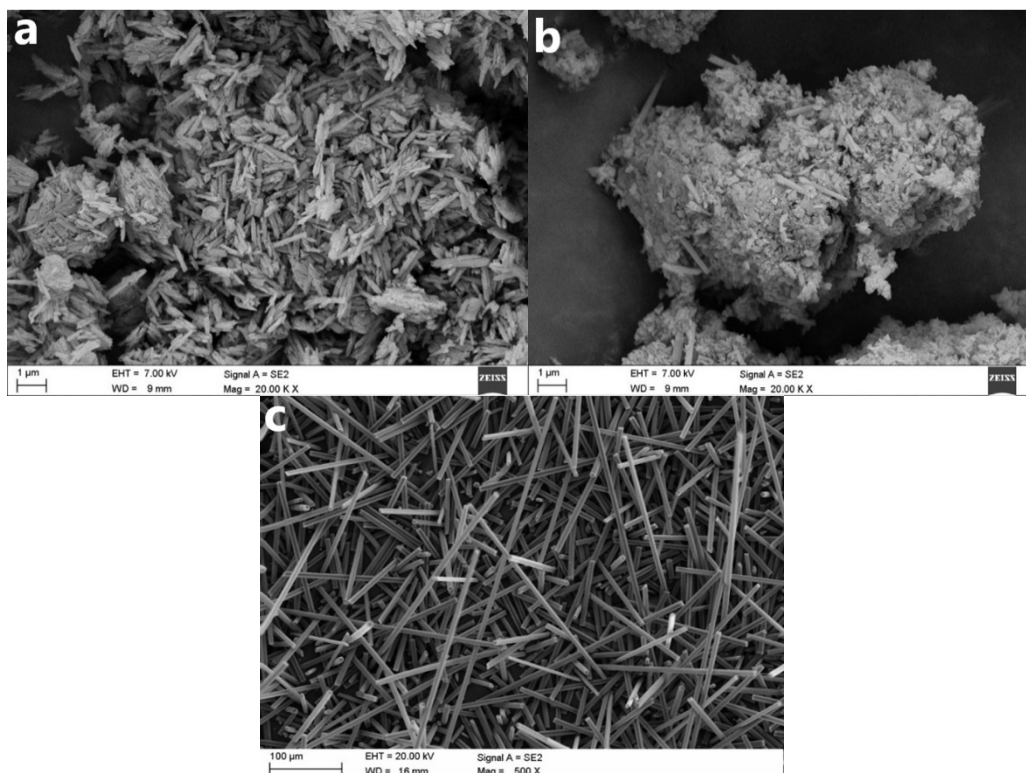


Fig. 1. Morphology of: a) pure halloysite (mag. 20,000x), b) Dunino halloysite (mag. 20,000x), c) carbon fibers (mag. 500x)

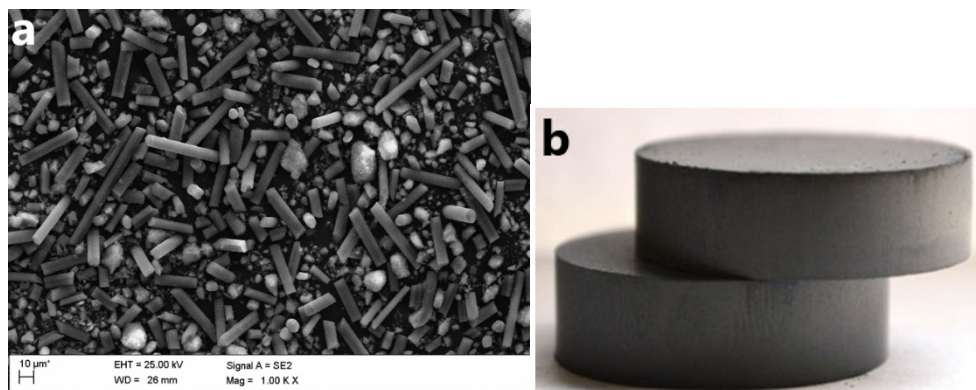


Fig. 2. a) Morphology of a mixture consisting of pure halloysite and carbon fibers (mag. 1,000x), b) green bodies

Green bodies of mixtures containing: 70 wt.% of pure halloysite, 30 wt.% carbon fibres and 1 wt.% microwax and 50 wt.% of pure halloysite, 50 wt.% of carbon fibres and 1 wt.% of microwax were obtained by grinding the blends for 15 minutes in a Fritsch ball mill, followed by uniaxial pressing at 100 MPa for 15 seconds (Fig. 2a). The 30 mm diameter and 10-mm thickness mouldings (Fig. 2b) were used for high-temperature microscopic observations so as to verify the sintering temperature range in order to obtain ceramic preforms as reinforcement.

The reinforcement in the form of a ceramic preform should have a porous structure allowing for full infiltration by liquid metal. Therefore, a production method that involved sintering halloysite with the addition of a pore-forming agent in the form of carbon fibres was selected [1,34]. These fibres undergo degradation at elevated temperatures (by-product of oxidation – CO<sub>2</sub>). The simplified scheme of obtaining porous ceramic skeletons is shown in Figure 3.

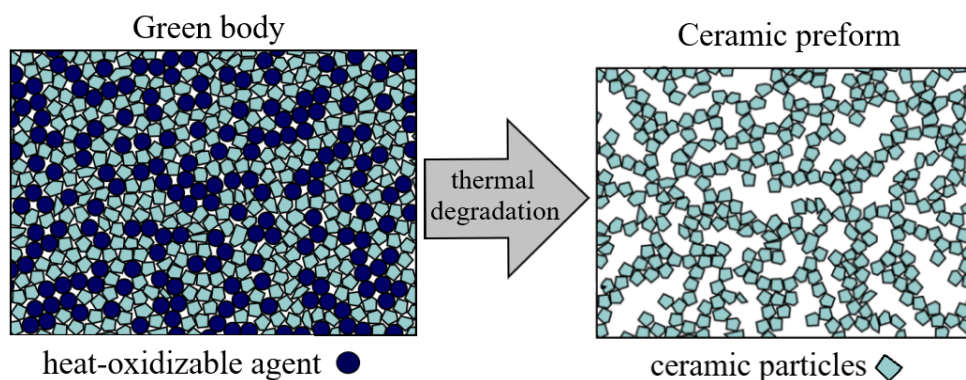


Fig. 3. The method of pore formation using a heat-oxidizable agent [37]

## 2.2. Testing methods

Research on thermal effects (DTA) and mass changes (TG/DTG) during heating of pure halloysite, Dunino halloysite and carbon fibres was performed in the MOM Q-1500D derivatograph. Samples of different weights, but with a similar volume, were heated at a constant speed (7.5°C/min) in the temperature range of 20-1500°C, in air atmosphere.

To simulate the phenomena taking place during the production of porous ceramic skeletons, investigations into the linear changes of pure halloysite, halloysite and mixtures versus temperature were carried out using the microscopic-photographic method, in a Leitz high-temperature microscope [35].

Samples placed on a corundum support were heated to 1500°C at a rate of 5°C/min in air atmosphere. Samples of pure and natural halloysite were pressed in a hand press in the form of cubes with a side of approx. 3 mm, while green body samples (50 wt.% CF and 30 wt.% CF) were cut out in the form of cubes having a side of ca 3 mm. During observations of the sample in the microscope eyepiece, the image of the sample was recorded at temperatures corresponding to changes in the shape of the sample (shrinkage, expansion). Thanks to continuous observation of the sample and photographic recording of changes in its shape and dimensions as a function of temperature, a number of photographs showing the behaviour of the material during heating were obtained. The relative change of the cross-sectional area of the sample  $\delta(T)$  (versus

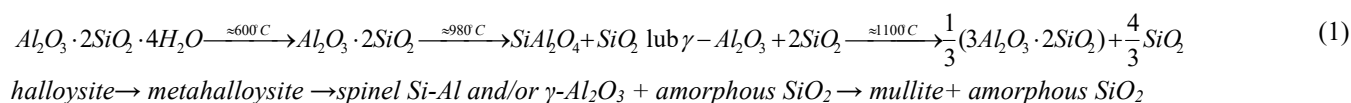
temperature) and characteristic temperatures were determined on the basis of the photos of the sample.

The qualitative analysis of the phase composition of pure halloysite in the initial state and after annealing at the temperature in the range of 100-1500°C was carried out using an X'Pert PRO X-ray diffractometer with Co K $\alpha$  radiation, produced by PANalytical. Phase identification was carried out using X'Pert HighScore Plus equipped with the ICDD file base -PDF - 4+.

The porosity analysis of the prepared ceramic preforms was performed based on the measurements of their geometry and mass.

## 3. Results and discussion

The result of DTA/TG/DTG analysis of pure halloysite is shown in Figure 4. In the temperature range of 60-75°C, an endothermic process associated with dehydration (adsorption water release, weight loss about 2 wt.%) is observed, whereas in the range of 400-600°C (maximum at 516°C) it is an endothermic process (dehydroxylation) related to the decomposition of halloysite to meta-halloysite (weight loss about 17 wt.%). At the temperature of approximately 980°C, an exothermic process related to the reconstruction of the halloysite structure and the formation of the Si-Al spinel phase as a transition form takes place [14,22,28,36], followed by structural transformation of halloysite into mullite (according to the simplified formula (1)) [14,16,17,20,21,26].



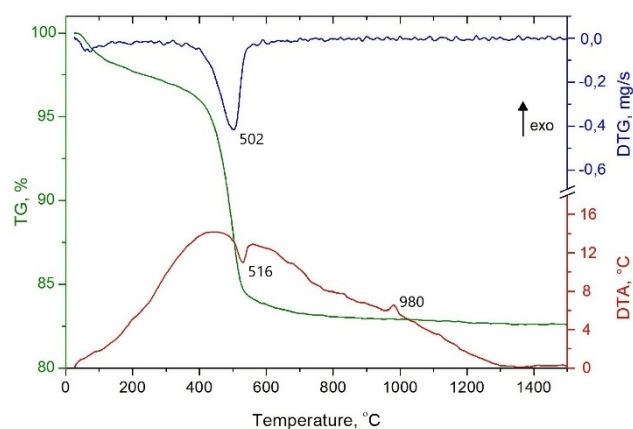


Fig. 4. TG/DTG and DTA curves for the pure halloysite (sample weight  $m_0=70$  mg)

The DTA/TG/DTG analysis of Dunino halloysite is shown in Figure 5. In the temperature range of 65–85°C, an endothermal process associated with halloysite dehydration (loss of mass about 2.5 wt.%) is observed, while in the temperature range of 450–550°C (maximum at 526°C) – an endothermal process associated with halloysite dehydroxylation and decomposition to meta-halloysite (loss of mass 20 wt.%).

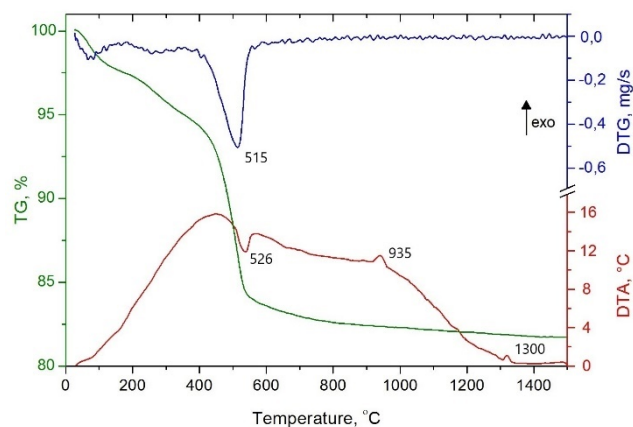


Fig. 5. TG/DTG and DTA curves for the Dunino halloysite (sample weight  $m_0=100$  mg)

At the temperature of ca. 935°C – an exothermic process takes place, which is connected with the rebuilding of the halloysite structure and the formation of the Si-Al spinel phase as a transition form, followed by the formation of mullite. The low exothermic peak at the temperature of approx. 1300°C is associated with secondary mullite, additionally, the characteristic temperature of the material

softening is also recorded. Although both halloysites show similar kinetics of phase transitions and chemical reactions, the differences in the content of impurities influence the mullitisation temperature: the reconstruction of Dunino halloysite structure begins at a temperature lower by ca 50°C than in the case of pure halloysite. However, a slightly higher loss of halloysite mass was observed in the range up to 400°C.

The addition of carbon fibres to halloysite was intended to slow weight loss and reduce the linear changes accompanying halloysite dehydroxylation. Therefore, the temperature range in which this effect may be the greatest was investigated. The DTA/TG/DTG result of carbon fibres presented in Figure 6, shows that the oxidation of carbon fibres (the factor determining the porosity in the ceramic skeleton, shrinkage inhibition) starts at approx. 400°C (the beginning of mass loss due to carbon oxidation, ca 3 wt.%). In the temperature range of approx. 570–772°C, the rate of oxidation reaction decreases. The total loss of mass was recorded at 775°C.

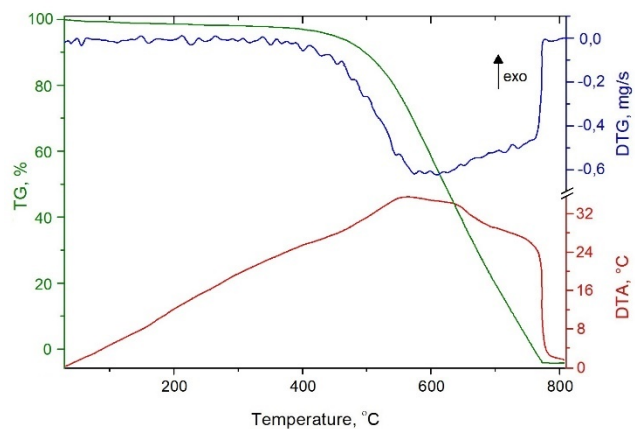


Fig. 6. TG/DTG and DTA curves for the carbon fibers (sample weight  $m_0=40$  mg)

Photos of samples of halloysite nanotubes and Dunino halloysite at selected temperatures, recorded under a high-temperature microscope and a graph of linear changes as a function of temperature, are shown in Figures 7 and 8.

Sintering of pure halloysite starts at temperatures above 600°C, while sintering of Dunino halloysite at temperatures close to 500°C. In the range of 600–1100°C, the rate of linear changes is similar in both cases. From 1200°C the sintering of HNT is characterized by a linear change of the cross-sectional area of the sample up to 1400°C.

The changes in the cross-sectional area of pure halloysite in the range up to 1100°C (Fig. 8) are related to the phenomena described in Eq. (1) and recorded in DTA/TG (Fig. 4).

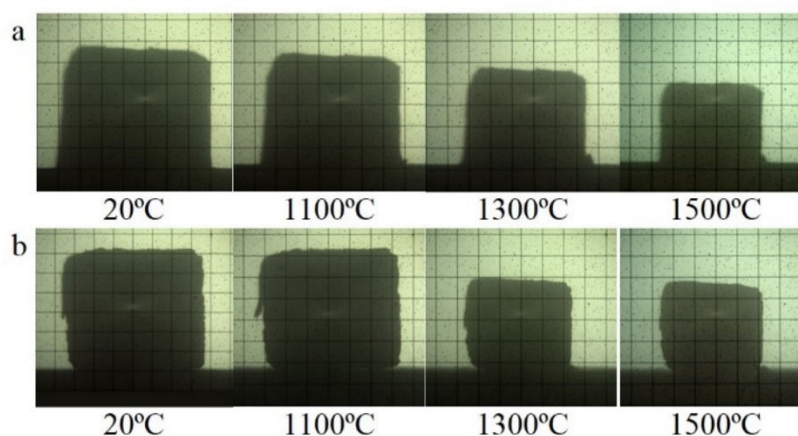


Fig. 7. Photos of a) pure and b) Dunino halloysite cube sample during the test in a high-temperature microscope

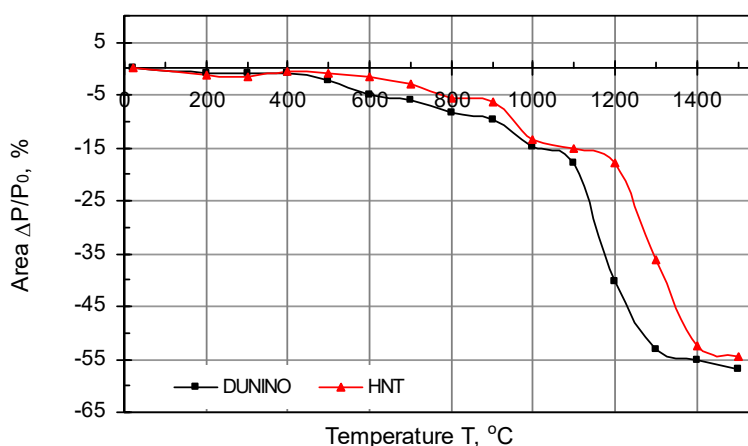


Fig. 8. Dimensional changes of Dunino halloysite (DUNINO) and pure halloysite (HNT), heating rate 5°C/min

The inflection point on the curve of linear changes of HNT (Fig. 8) at the temperature of ca 1000-1100°C is related to the transition of meta-halloysite to mullite through an amorphous phase. At a temperature of approx. 1100°C a structure consisting of  $\gamma$ -Al<sub>2</sub>O<sub>3</sub> crystals deposited in the amorphous phase of silica was obtained (Fig. 9) [16,22,23].

The changes of the cross-sectional area of Dunino halloysite up to 1000°C shown in Figure 8 are related to the effects described in Eq. (1) and recorded in the DTA/TG study (Fig. 5). From 1100°C to 1300°C, the sintering of halloysite is characterized by a linear change in the cross-sectional area of the sample. At 1300°C the sample begins to soften (impurities in the Dunino halloysite induce a liquid phase during firing). The shift of the beginning of sintering to lower temperatures compared to the sintering of nanotubes as well as the emergence of a liquid phase may be due to the presence of impurities (Tab. 1). The presence of more

than 1 wt.% Fe<sub>2</sub>O<sub>3</sub> in the mullite material causes a shift in the softening temperature towards lower temperatures and an increase in the rate of sintering and mullitisation [31-33]. While it is economically desirable to lower the sintering and mullitisation temperature, lowering the softening temperature of porous ceramic preforms leads to deformation of the structure as a result of too fast and uneven volume changes. Therefore, the use of Dunino halloysite has been abandoned in this experiment due to the difficulty in obtaining a homogenous shrinkage across the entire sample volume.

DTA/TG and high-temperature microscopy investigations of pure halloysite were complemented with a qualitative analysis of the phase composition of HNT preheated at various temperatures (Fig. 9). During the heating of pure halloysite, the characteristic changes of the structure were observed at the temperature of 1100°C and 1500°C.

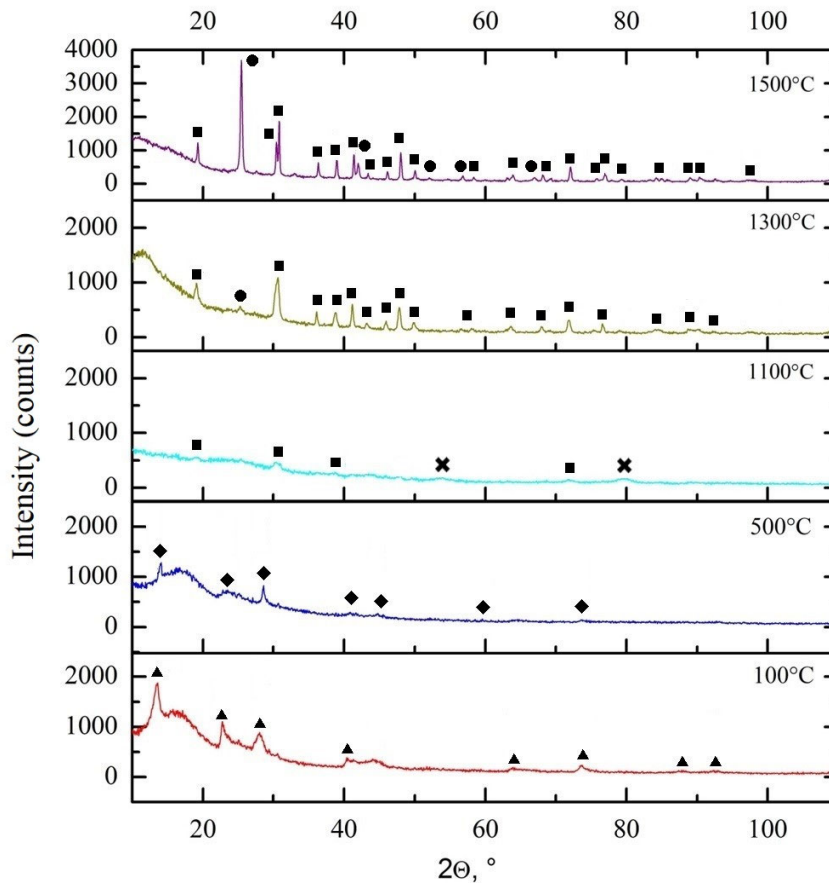
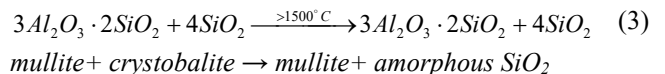
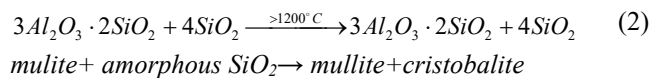


Fig. 9. XRD patterns of sintered specimens at 100, 500, 1100, 1300, 1500°C (▲ hydrohalloysite, ◆ meta-halloysite, ✕  $\gamma$ - $\text{Al}_2\text{O}_3$ , ■ mullite, ● cristobalite)

HNT heated at 1100°C is characterized by an amorphous structure with  $\gamma$ - $\text{Al}_2\text{O}_3$  phase separations [23] (the Al-Si spinel phase cannot be excluded because of difficulties in distinguishing the two phases due to their similar crystalline structure and close crystal network parameters [37]). The beginning of mullite crystallization was also identified.

Mullite and cristobalite were found in the samples heated at 1300°C and 1500°C (Fig. 9). At temperatures above 1200°C, cristobalite is formed as a result of crystallisation of microcrystalline silica (mainly amorphous [38]), according to Eq. (2). As shown in [39], it is possible to obtain the mullite structure without crystallisation of cristobalite by increasing the heating rate. Heating at temperatures higher than 1500°C was not taken into account due to the conversion of cristobalite into amorphous silica in accordance with Eq. (3), which reduces the density of the obtained material and, in consequence, its properties, so this temperature would also have no economic reason [14,40].



Based on DTA/TG, high-temperature microscopy and phase analysis results, pure halloysite was selected for further research. Mixtures of HNT, carbon fibres and microwax were used to prepare samples for the simulation of green bodies sintering in a high-temperature microscope. Photographs of green bodies samples with 50 wt.% and 30 wt.% carbon fibres taken at selected temperatures during the investigations in a high-temperature microscope are shown in Figure 10. The graph of linear changes versus temperature is shown in Figure 11.

It has been shown that the percentage by weight of carbon fibres in mixtures has no effect on limiting the changes in sample size in the range up to 1400°C compared

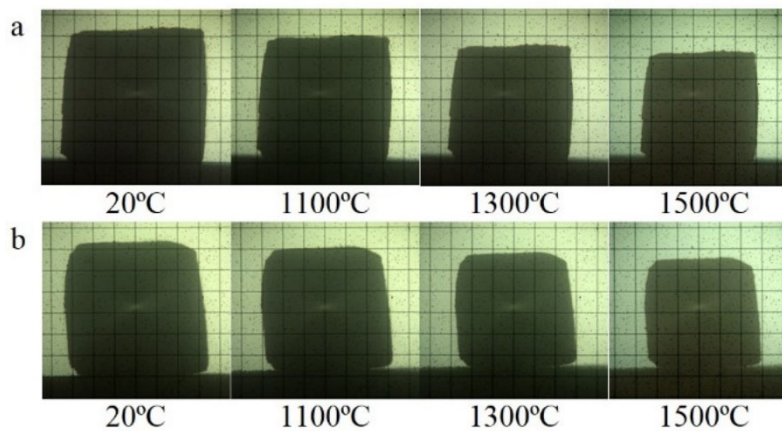


Fig. 10. Photos of green bodies consisting of a) HNT (50 wt.%) and carbon fibres (50 wt.%), b) HNT (70 wt.%) and carbon fibres (30 wt.%), during the test in a high-temperature microscope

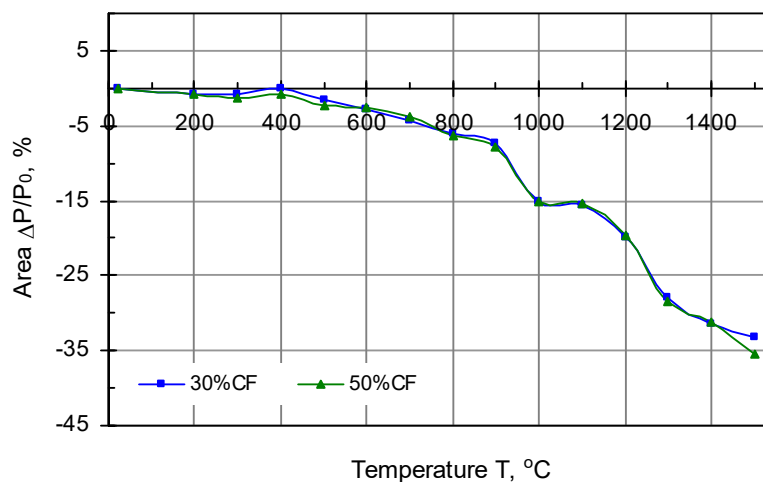


Fig. 11. Changes in the dimensions of the green body from HNT and 30 wt.% and 50 wt.% CF, heating rate 5°C/min

to the changes observed for HNT samples (Fig. 11). The rate of linear changes is the same up to 1400°C. However, the presence of fibres in green bodies significantly reduces the velocity of linear changes in the temperature above 1200°C, compared to the changes recorded for HNT (Fig. 8).

Thermal investigations of pure halloysite and its green bodies with carbon fibre revealed characteristic temperatures of 1200°C and 1400°C in the course of sintering. Therefore, the green bodies were sintered at 1100°C, 1300°C and 1500°C to examine the properties of ceramic skeletons obtained at these temperatures [23]. Since the high-temperature microscope uses cubic samples cut from green bodies with a side of about approx. 3 mm, so these samples cannot be used as representative ones because it is impossible to estimate the content of carbon fibres in the mixture. The properties of the porous ceramic skeletons

obtained are given in Table 2, while the morphology of their fractures an view is shown in Figure 12.

The share of pores and the share of mass ceramic phase in a sintered mixture at the temperature of 1500°C are much more differentiated. For mixtures sintered at temperatures of 1100°C and 1300°C, this effect is similar: an increase in the content of fibres leads to a decrease in apparent density and in the share of ceramic phase, and, at the same time, to a decrease in the weight of the sample after sintering. The influence of the fibre content in sintered parts on the physical properties of the preforms at the temperatures of 1100°C, 1300°C and 1500°C is confirmed by the lack of homogeneity of the sample visible in high-temperature microscopic investigations.

Further experiments (pressure infiltration, research on AlSi12-mullite composites) not being the subject of this publication showed that, from the practical point of view, the



Table 2.  
Physical properties of sintered ceramic preforms

CF, wt.%	Weight $m_p$ , g	Apparent density $\rho$ , g/cm <sup>3</sup>	Pores, %	Ceramic phase, %
Sintering temperature 1100°C				
50	3.46	0.67	77.59	22.41
30	5.05	1.00	66.54	33.46
Sintering temperature 1300°C				
50	3.1	0.94	68.79	31.21
30	4.91	1.32	55.88	44.12
Sintering temperature 1500°C				
50	2.8	0.93	69.14	30.86
30	4.4	1.54	48.72	51.28

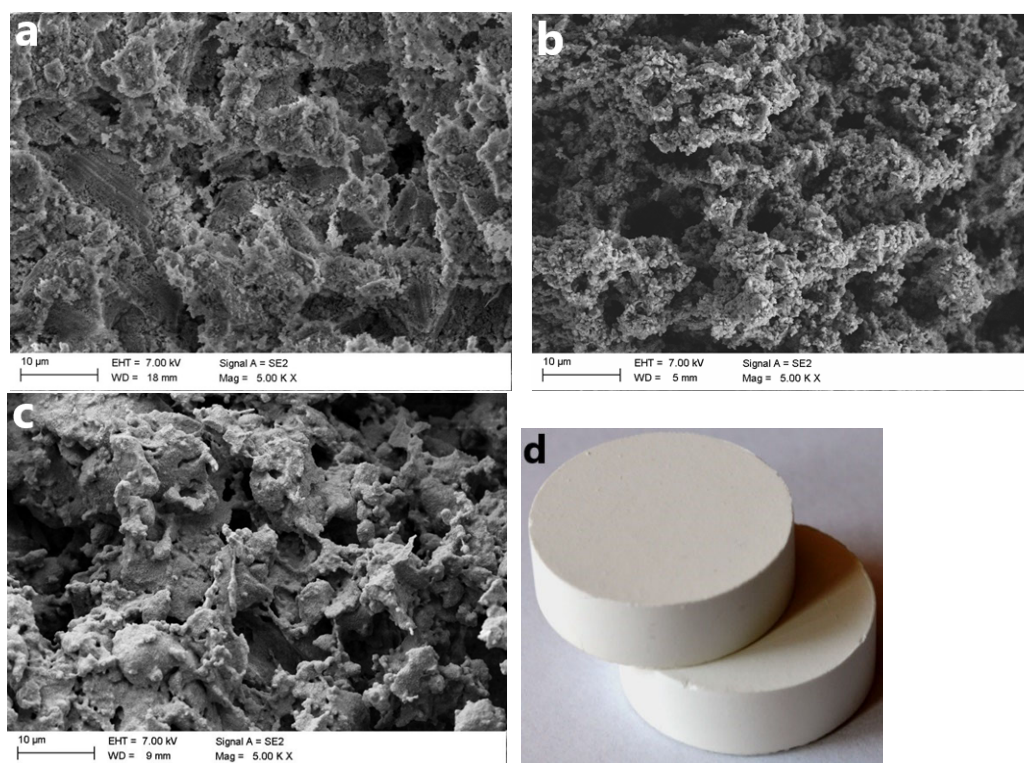


Fig. 12. Morphology of porous ceramic skeletons sintered at: a) 1100°C, b) 1300°C, c) 1500°C, d) sintered preforms

sintering temperature of 1100°C is not sufficient to produce porous ceramic preforms with properties enabling their subsequent application (pressure and gas infiltration with a liquid alloy) due to their high brittleness, low cohesion and low strength properties [23].

#### 4. Conclusions

The results indicate that:

1. Dunino halloysite cannot be used for the production of sintered, porous ceramic preforms due to the presence of

impurities, which shifted the sintering temperature towards lower temperatures and caused a rapid shrinkage of the sample above 1200°C and the appearance of the softening temperature at 1300°C.

2. Thermal studies (DTA/TG, linear changes in high-temperature microscopy) confirmed the possibility of using pure halloysite to manufacture the reinforcement for metal matrix composites, and the addition of fibres allowed obtaining a porous structure of the reinforcement. Free sintering of mouldings of mixtures of pure halloysite and carbon fibres within the temperature range resulting from the analysis of thermal investigations

enabled obtaining porous ceramic preforms having a mullite structure with cristobalite precipitations and porosity within the range of ca 49-78%.

3. The assessment of the impact of carbon fibres on the porous structure of sintered halloysite was possible only in the case of green bodies heated at the temperatures of 1100°C, 1300°C and 1500°C. The selection of the temperature of these green bodies heat treatment was based on the results of high-temperature microscopic investigations. The analysis of the phase composition of the sintered parts confirmed the correct choice of the sintering temperatures.

## References

- [1] L.A. Dobrzański, G. Matula, A.D. Dobrzańska-Danikiewicz, P. Malara, M. Kremzer, B. Tomiczek, M. Kujawa, E. Hajduczek, A. Achteik-Franczak, L.B. Dobrzański, J. Krzysieczko, Composite materials infiltrated by aluminium alloys based on porous skeletons from alumina, mullite and titanium produced by powder metallurgy techniques, in: L.A. Dobrzański (ed.), *Powder Metallurgy – Fundamentals and Case Studies*, InechOpen, Rijeka, Croatia, 2017, 95-137. DOI: <http://dx.doi.org/10.5772/65377>
- [2] K.M. Sree Manu, L. Ajay Raag, T.P.D. Rajan, Manoj Gupta, B.C. Pai, Liquid metal infiltration processing of metallic composites: a critical review, *Metallurgical and Materials Transactions B* 47 (2016) 2799-2819. DOI: <https://doi.org/10.1007/s11663-016-0751-5>
- [3] K. Lades, Piston useful for an internal combustion engine, preferably for gasoline engine, comprises ring groove, which is designed with infused reinforcement comprising metal infiltrated, preferably steel- and/or gray cast-infiltrated ceramic, DE102012214910A1.
- [4] P. Długosz, P. Darlak, Manufacture of lightweight components for a composite protective armour using squeeze casting technologies, *Fast Tracked Vehicles* 38/3 (2015) 141-162.
- [5] P. Dudek, P. Darlak, P. Długosz, A. Fajkiel, Porous ceramic preforms dedicated for local reinforcement subjected to the squeeze casting infiltration process, *Maintenance Problems* 3 (2015) 75-82.
- [6] L.A. Dobrzański, M. Kremzer, A. Nagel, B. Huchler, Fabrication of ceramic preforms based on Al<sub>2</sub>O<sub>3</sub> CL 2500 powder, *Journal of Achievements of Materials and Manufacturing Engineering* 18/1-2 (2006) 71-74.
- [7] L.A. Dobrzański, M. Kremzer, A. Nagel, Structure and properties of ceramic preforms based on Al<sub>2</sub>O<sub>3</sub> particles, *Journal of Achievements in Materials and Manufacturing Engineering* 35/1 (2009) 7-13.
- [8] K. Naplocha, K. Granat, The structure and properties of hybrid preforms for composite, *Journal of Achievements in Materials and Manufacturing Engineering* 22/2 (2007) 35-38.
- [9] M. Potoczek, R.E. Śliwa, J. Myalski, J. Śleziona, Metal-ceramic interpenetrating composites produced by pressure infiltration of metal into ceramic foams, *Ores and Non-Ferrous Metals* 54/11 (2009) 688-692.
- [10] A.J. Dolata, M. Dyzia, Z. Jaegermann, Structure and physical properties of alumina ceramic foams designed for centrifugal infiltration process, *Composites Theory and Practice* 17/3 (2017) 136-143.
- [11] N. Sobczak, L. Jaworska, M. Podsiadło, B. Smuk, R. Nowak, P. Kurtyka, A. Twardowska, Nitride and carbide preforms for infiltration process, *Archives of Materials Science and Engineering* 28/11 (2007) 653-656.
- [12] B. Tomiczek, M. Kujawa, G. Matula, M. Kremzer, T. Tański, L.A. Dobrzański, Aluminium AlSi12 alloy matrix composites reinforced by mullite porous preforms, *Materialwissenschaft und Werkstofftechnik* 46/4-5 (2015) 368-376. DOI: <https://doi.org/10.1002/mawe.201500411>
- [13] J. Guan, L. Qi, J. Liu, J. Zhou, X. Wei, Threshold pressure and infiltration behavior of liquid metal into fibrous preform, *Transactions of Nonferrous Metals Society of China* 23/11 (2013) 3173-3179. DOI: [https://doi.org/10.1016/S1003-6326\(13\)62849-6](https://doi.org/10.1016/S1003-6326(13)62849-6)
- [14] C.Y. Chen, G.S. Lan, W.H. Tuan, Microstructural evolution of mullite during the sintering of kaolin powder compacts, *Ceramics International* 26/7 (2000) 715-720. DOI: [https://doi.org/10.1016/S0272-8842\(00\)00009-2](https://doi.org/10.1016/S0272-8842(00)00009-2)
- [15] C. Venturelli, M. Paganelli, Sintering behaviour of clays for the production of ceramics, *Process Engineering* 84/5 (2007) 1-4.
- [16] P. Yuan, D. Tan, F. Annabi-Bergaya, W. Yan, M. Fan, D. Liu, H. He, Changes in structure, morphology, porosity, and surface activity of mesoporous halloysite nanotubes under heating, *Clays and Clay Minerals* 60/6 (2012) 561-573. DOI: <https://doi.org/10.1346/CCMN.2012.0600602>
- [17] D.J. Duval, S.H. Risbud, J.F. Shackelford, Mullite, in: J.F. Shackelford, R.H. Doremus (eds.), *Ceramic and Glass Materials*, 2008.
- [18] H. Schneider, S. Komarneni, *Mullite*, Wiley-VCH, Weinheim, 2005.
- [19] P. Taźbierski, C. Dziubak, A. Oziębło, Mullite powder synthesis by solid state reaction in powder bed, *Glass and Ceramics* 66/4 (2015) 21-23 (in Polish).
- [20] L. Andrini, R. Moreira Toja, M.S. Conconi, F.G. Requejo, N.M. Rendtorff, Halloysite nanotube and its firing products: Structural characterization of halloysite, metahalloysite, spinel type silicoaluminate

- and mullite, *Journal of Electron Spectroscopy and Related Phenomena* 234 (2019) 19-26. DOI: <https://doi.org/10.1016/j.elspec.2019.05.007>
- [21] A.K. Chakraborty, DTA study of preheated kaolinite in the mullite formation region, *Thermochimica Acta* 398/1-2 (2004) 203-209. DOI: [https://doi.org/10.1016/S0040-6031\(02\)00367-2](https://doi.org/10.1016/S0040-6031(02)00367-2)
- [22] J. Ouyang, Z. Zhou, Y. Zhang, H. Yang, High morphological stability and structural transition of halloysite (Huan, China) in heat treatment, *Applied Clay Science* 101 (2014) 16-22. DOI: <https://doi.org/10.1016/j.clay.2014.08.010>
- [23] M. Kujawa, Infiltrated aluminium alloy matrix composites reinforced with sintered halloysite nanotubes, PhD thesis, Silesian University of Technology, Gliwice, Poland, 2015.
- [24] M. Kujawa, L.A. Dobrzański, G. Matula, M. Kremzer, B. Tomiczek, Manufacturing of Porous Ceramic Preforms Based on Halloysite Nanotubes (HNTs), *Archives of Metallurgy and Materials* 61/2B (2016) 917-922. DOI: <https://doi.org/10.1515/amm-2016-0155>
- [25] S. Hillier, R. Brydson, E. Delbos, T. Fraser, N. Gray, H. Pendrowski, I. Phillips, J. Robertson, I. Wilson, Correlations among the mineralogical and physical properties of halloysite nanotubes (HNTs), *Clay Minerals* 51/3 (2016) 325-350. DOI: <https://doi.org/10.1180/claymin.2016.051.3.11>
- [26] H. Schneider, J. Schreuer, B. Hildmann, Structure and properties of mullite - a review, *Journal of the European Ceramic Society* 28/2 (2008) 329-344. DOI: <https://doi.org/10.1016/j.jeurceramsoc.2007.03.017>
- [27] J. Lis, R. Pampuch, Sintering, The AGH University of Science and Technology Press, Cracow, 2000.
- [28] P. Yuan, D. Tan, F. Annabi-Bergaya, Properties and applications of halloysite nanotubes: recent research advances and future prospects, *Applied Clay Science* 112-113 (2015) 75-93. DOI: <https://doi.org/10.1016/j.clay.2015.05.001>
- [29] P. Yuan, A. Thill, F. Bergaya (eds.), Nanosized tubular clay minerals: halloysite and imogolite, Elsevier, Amsterdam, 2016.
- [30] M. Lutyński, P. Sakiewicz, S. Lutyńska, Characterization of diatomaceous earth and halloysite resources of Poland, *Minerals* 9/11 (2019) 670. DOI: <https://doi.org/10.3390/min9110670>
- [31] R. Ceylantekin, R. Başar, Solid solution limit of  $\text{Fe}_2\text{O}_3$  in mullite crystals, produced from kaolin by solid state reactions, *Ceramics International* 44/7 (2018) 7599-7604. DOI: <https://doi.org/10.1016/j.ceramint.2018.01.178>
- [32] K.O. Ajanaku, O. Aladesuyi, M. Pal, S.K. Das, Evaluation of Nigerian source of kaolin as a raw material for mullite synthesis, *Oriental Journal of Chemistry* 32/3 (2016) 1571-1582. DOI: <http://dx.doi.org/10.13005/ojc/320333>
- [33] W.E. Lee, G.P. Souza, C.J. McConville, T. Tarvornpanich, Y. Iqbal, Mullite formation in clays and clay-derived vitreous ceramics, *Journal of the European Ceramic Society* 28/2 (2008) 465-471. DOI: <https://doi.org/10.1016/j.jeurceramsoc.2007.03.009>
- [34] B.A. Huchler, Pressure infiltration behaviour and properties of aluminium alloy - Oxide ceramic preform composites, PhD thesis, University of Birmingham, Birmingham, United Kingdom, 2009.
- [35] R. Suwak, High temperature microscope research, *Refractory Materials* 2 (2015) 43-48.
- [36] E. Joussein, S. Petit, C. Fialips, P. Vieillard, D. Righi, Differences in the dehydration-rehydration behavior of halloysites: New evidence and interpretations, *Clays and Clay Minerals* 54/4 (2006) 473-484. DOI: <https://doi.org/10.1346/CCMN.2006.0540408>
- [37] Y. Wang, H. Liu, H. Cheng, J. Wang, Densification behavior and microstructure of mullite obtained from diphasic  $\text{Al}_2\text{O}_3$ - $\text{SiO}_2$  gels, *Ceramics International* 40/8B (2014) 12789-12796. DOI: <https://doi.org/10.1016/j.ceramint.2014.04.133>
- [38] M.V.M. Magliano, V.C. Pandolfelli, Refractories mullitization with different sources of reactants - review, *Cerâmica* 56/340 (2010) 368-375. DOI: <https://doi.org/10.1590/S0366-69132010000400009>
- [39] K.C. Liu, G. Thomas, Time-temperature-transformation curves for kaolinite  $\alpha$ -alumina, *Journal of the American Ceramic Society* 77/6 (1994) 1545-1552. DOI: <https://doi.org/10.1111/j.1151-2916.1994.tb09755.x>
- [40] P.C. Yu, Y.W. Tsai, F.S. Yen, C.L. Huang, Thermal reaction of cristobalite in nano  $\text{SiO}_2/\alpha\text{-Al}_2\text{O}_3$  powder systems for mullite synthesis, *Journal of the American Ceramic Society* 97/8 (2014) 2431-2438. DOI: <https://doi.org/10.1111/jace.12989>



© 2021 by the authors. Licensee International OCSCO World Press, Gliwice, Poland. This paper is an open access paper distributed under the terms and conditions of the Creative Commons Attribution-NonCommercial-NoDerivatives 4.0 International (CC BY-NC-ND 4.0) license (<https://creativecommons.org/licenses/by-nc-nd/4.0/deed.en>).